https://doi.org/10.5194/egusphere-2026-4218
Preprint. Discussion started: 4 August 2026

Multi-Rotor UAV Observations of the Atmospheric Boundary Layer over Complex Terrain: Accuracy Validation and Dynamic Mechanisms of Flight Disturbances

Rongfang Yang[1,2], Deli Meng[3], Guanglei Zhang[4] ,Lihui Liu[5], Guocui Li[6], Zhen Zhang[7*],Jianping Guo[7,8*]

[1] China Meteorological Administration Xiong'an Atmospheric Boundary Layer Key Laboratory, Hebei, China

[2] Hebei Provincial Meteorological Information Center, Hebei, China

[3] National Institute of Natural Hazards Prevention, Beijing, China

[4] Beijing HY Orient Detection Technology Co., Ltd., Beijing 100081, China;

[5] Xingtai Meteorological Bureau, Hebei, China

[6] Shijiazhuang Meteorological Bureau, Hebei, China

[7] State Key Laboratory of Severe Weather Meteorological Science and Technology & Special Meteorological Advanced Support Technology Research Center, Chinese Academy of Meteorological Sciences, Beijing, China

[8] Field Scientific Experiment Base for Meteorological Support of Low-Altitude Economy Unmanned Aerial Vehicles, Guangdong-Hong Kong-Macao Greater Bay Area, China Meteorological Administration, Guangdong, China

Correspondence to: Dr/ Prof. Jianping Guo (Email: jpguocams@gmail.com) and Zhen Zhang (Email: mailto:zhangzhencams@outlook.com)

https://doi.org/10.5194/egusphere-2026-4218
Preprint. Discussion started: 4 August 2026

Abstract

Unmanned aerial vehicle (UAV)-based sounding has become a flexible and cost-effective approach for probing the atmospheric boundary layer (ABL), yet its measurement credibility over complex terrain and the dynamic response of UAV flight attitude to boundary-layer dynamics remain insufficiently quantified. Here, we implement multi-rotor UAV field campaigns equipped with well-calibrated meteorological payloads, including co-located intercomparison observations against a 100-m gradient meteorological tower at the Xingtai Field Scientific Experiment Base, and vertical-profile surveys across the lower ABL over the eastern Taihang piedmont. The comparative observations demonstrate excellent agreement between UAV and tower measurements: vertical profiles of wind speed, wind direction, air temperature, and relative humidity exhibit strong correlations, negligible systematic biases, and coherent vertical structures. Stability parameters derived from high-frequency hovering observations, including potential temperature and gradient Richardson number (Ri), also closely match tower references, verifying the platform's capability to reliably resolve ABL thermal stratification and dynamic stability. Three successive evening soundings capturing the transition from a convective to a stable boundary layer reveal that UAV attitude disturbances are strongly suppressed within stably stratified layers, but markedly amplified in near-neutral to weakly unstable layers where intense vertical wind shear coincides with weak thermal suppression, with the most severe perturbations occurring near the cloud base. The joint distribution of Ri and vertical wind shear further indicates that turbulence-induced flight bumpiness generally intensifies with increasing shear and peaks under unstable stratification, while a localized anomaly suggests possible resonance-like coupling between turbulent eddy scales and airframe dynamics. These findings establish a quantitative observational basis for reliable UAV-based ABL sensing and low-altitude flight-safety assessment over complex terrain.

https://doi.org/10.5194/egusphere-2026-4218
Preprint. Discussion started: 4 August 2026

1 Introduction

Through turbulent exchange of momentum, heat, water vapour, aerosols, and trace gases, the ABL regulates near-surface weather evolution, cloud and fog formation, and the meteorological environment experienced by low-altitude operations (Stull, 1988; Garratt, 1992; Wulfmeyer et al., 2015). Its most dynamically active portion commonly lies within the lowest several hundred metres to approximately 1–2 km above ground level, where wind shear, thermal stratification, and turbulent mixing can change rapidly over minutes to hours and over short horizontal distances (Seibert et al., 2000; Stith et al., 2018). Accurate, vertically resolved observations in this layer are therefore essential for boundary-layer parameterization, numerical weather prediction, air-quality assessment, and low-level flight-safety evaluation.

Despite this importance, the lower ABL remains structurally under-sampled by conventional observing systems. Surface meteorological stations provide long-term and reliable measurements, but they represent only fixed points near the ground and cannot resolve the vertical gradients that determine boundary-layer stability and turbulence. Radiosondes provide vertical profiles of temperature, humidity, pressure, and wind, yet their launches are typically sparse in time and space; once released, the balloon drifts passively with the ambient flow and cannot repeatedly sample a prescribed location or be recovered for targeted near-surface profiling (Seibert et al., 2000; Stith et al., 2018). Meteorological towers, wind profilers, radar, and lidar systems can partly improve vertical coverage, but their deployment is constrained by fixed siting, installation and maintenance costs, minimum detectable range, terrain dependence, and reduced representativeness away from the instrument location (Illingworth et al., 2019; Wulfmeyer et al., 2015). As a result, a persistent observational gap exists between near-surface point measurements and coarser upper-air or remote-sensing observations, particularly in the lowest 1–2 km where boundary-layer structure is most relevant to weather, pollution, and low-altitude activity. Filling this gap requires an observing approach capable of providing flexible, repeatable, and vertically resolved in-situ measurements within the lower atmosphere.

Unmanned aerial vehicles (UAVs) provide a practical means of reducing this observational gap because they can obtain targeted in-situ measurements in layers that are difficult to sample repeatedly with conventional platforms. Their mobility, relatively low operational cost, and

https://doi.org/10.5194/egusphere-2026-4218
Preprint. Discussion started: 4 August 2026

flexible deployment allow observations to be conducted over heterogeneous underlying surfaces, complex terrain, and rapidly evolving boundary-layer conditions. Over the past two decades, UAV-based atmospheric measurements have been used to characterize temperature and humidity profiles, turbulence, aerosols, trace gases, and urban or polar boundary-layer processes, demonstrating their value as an intermediate observing platform between fixed ground stations and conventional upper-air soundings (Cassano, 2014; Hobbs et al., 2002; Jonassen et al., 2015; Mamali et al., 2018; Reuder et al., 2012; Shelekhov et al., 2022). Recent studies have further shown that UAVs can provide high-resolution measurements of aerosol distributions and pollutant-related variables in the lower atmosphere, where vertical gradients are often strongest but least constrained by routine networks (Li et al., 2022; Pusfitasari et al., 2023; Weber et al., 2017).

Different UAV configurations, however, are suited to different observational objectives. Fixed-wing platforms offer longer endurance and broader horizontal coverage, making them useful for transects and regional surveys, but they generally require forward motion, larger operating space, and more complex flight paths when profiling a fixed column of air. Multi-rotor UAVs, by contrast, can take off and land vertically, hover at prescribed altitudes, and operate from confined sites without runways. These capabilities make them particularly suitable for fine-scale, layer-by-layer sounding of the lower ABL, where repeated measurements at selected heights are required to resolve vertical gradients of wind, temperature, humidity, and stability. Multi-rotor platforms have also been used to estimate low-altitude wind fields from onboard flight and attitude information, further extending their usefulness for boundary-layer observation when equipped with meteorological sensors (Palomaki et al., 2017; Wang et al., 2018). Therefore, for applications requiring vertically resolved, site-focused, and repeatable in-situ observations within the lower atmosphere, multi-rotor UAVs represent an appropriate observational choice.

Several studies have made important progress in validating UAV-based meteorological measurements. For wind observations, Shimura et al. (2018) compared hexarotor-derived wind profiles with tower observations and demonstrated the feasibility of wind-vector retrieval up to approximately 1000 m above the surface. Wetz et al. (2021) further showed that multiple quadrotor UAVs could provide distributed wind measurements in the ABL with good agreement against a 99 m tower. For thermodynamic measurements, Chang et al. (2020) developed an

https://doi.org/10.5194/egusphere-2026-4218
Preprint. Discussion started: 4 August 2026

optimized multicopter sounding technique and emphasized that sensor response delay can affect temperature and humidity profiles during ascent and descent. At the campaign scale, Barbieri et al. (2019) intercompared multiple small UAVs and showed that measurement quality depends strongly on sensor configuration, aspiration, radiation shielding, and platform integration. These studies collectively demonstrate that UAVs can provide useful lower-atmospheric observations when appropriately configured and calibrated.

However, existing validation efforts still leave several limitations. First, many comparisons have been conducted over relatively flat or horizontally homogeneous terrain, where flow distortion, thermal heterogeneity, and local circulations are less complex than in mountainous or terrain-transition regions. Second, validation has often focused on either a single reference height or a limited vertical range, whereas boundary-layer applications require confidence across multiple levels. Third, many studies have emphasized one category of variables, such as wind or thermodynamic profiles, rather than jointly evaluating wind speed, wind direction, temperature, humidity, and pressure together with derived stability-related parameters. Parameters such as potential temperature and the gradient Richardson number are especially important because they are not directly measured but are calculated from multiple basic variables; their uncertainty therefore accumulates from both sensor error and vertical-gradient estimation. Consequently, a key unresolved issue is whether a multi-rotor UAV can provide accurate, internally consistent measurements of both conventional meteorological elements and derived ABL parameters across multiple heights over complex terrain. Addressing this gap is a prerequisite for using UAV observations not only as descriptive profiles, but also as quantitative evidence for boundary-layer stability and turbulence analysis.

UAV observations are especially valuable in mountains, plateaus, glaciers, polar regions, and other station-sparse environments, where complex terrain and heterogeneous surfaces produce boundary-layer structures that are difficult to capture with fixed or routine observing systems (Zhou et al., 2025; Groos et al., 2025; Hansche et al., 2023; Jonassen et al., 2015). Yet these are also the environments in which strong vertical wind shear, terrain-induced turbulence, gravity-wave disturbances, and localized updrafts or downdrafts most frequently occur. Such dynamic forcing acts directly on multi-rotor aircraft, perturbing pitch, roll, yaw, angular velocity, and vertical acceleration, and therefore affects both flight safety and platform stability (Wang et al., 2019).

This coupling is particularly important because multi-rotor wind retrieval often depends on aircraft attitude or control-response information (Palomaki et al., 2017; Wang et al., 2018). Thus, atmospheric disturbances do not merely shake the platform; they can also contaminate the meteorological signal inferred from the platform response itself. Existing studies have commonly treated measurement accuracy and flight stability as separate issues, leaving insufficient evidence on how vertical wind shear and stratification stability jointly regulate UAV attitude disturbances under complex-terrain conditions. In particular, quantitative thresholds for stable operation remain poorly constrained. A co-located, synchronized analysis of the environment–attitude coupling is therefore necessary for both reliable UAV-based ABL observation and safe low-altitude deployment.

Motivated by these two gaps, this study investigates both the measurement performance and the environment–platform coupling of a multi-rotor UAV for ABL observation over complex terrain. Specifically, we aim to: (1) systematically evaluate the accuracy of UAV-derived conventional meteorological variables and stability-related parameters through co-located comparison with a gradient meteorological tower; and (2) clarify how vertical wind shear and stratification stability jointly modulate UAV attitude disturbances and identify quantitative thresholds for stable operation. The analysis relies on fixed-point hovering and vertical-profile observations collected during field campaigns at the Xingtai Field Scientific Experiment Base of the China Meteorological Administration, together with mountain sounding observations in Qianxian Township, Hebei Province. The remainder of this paper describes the observational platforms and methods, presents the accuracy validation and attitude-response analysis, and finally summarizes the implications for UAV-based ABL sensing and low-altitude flight-safety assessment.

2 Meteorological observations and methods

2.1 Gradient wind tower and UAVs measurements

The meteorological tower at the experimental base is used to provide benchmark data for the in-situ comparative verification of UAV-mounted meteorological sensors (Figure 1a). The

https://doi.org/10.5194/egusphere-2026-4218
Preprint. Discussion started: 4 August 2026

tower is vertically equipped with 10 observation layers at heights of 1 m, 2 m, 4 m, 8 m, 16 m, 32 m, 48 m, 64 m, 80 m and 96 m AGL, enabling minute-level vertical gradient observations of air temperature, relative humidity, wind direction, wind speed, atmospheric pressure, and three-dimensional ultrasonic wind within the ABL.

And a DJI MATRICE 350 RTK quadrotor UAV was deployed for all detection missions (Figure 1b). The UAV platform has a maximum ascent speed of 6 m/s, a maximum descent speed of 5 m/s, a maximum flight altitude of 5000 m, a maximum tolerable wind speed of 12 m/s, and an endurance time up to 55 minutes. Prior to the field campaigns, laboratory metrological calibration was conducted on the UAV-borne temperature, humidity, pressure, and wind sensors. The measurement errors at all calibration points were lower than the specified qualified thresholds, with no obvious data drift or missing records observed. The calibration results verify that the equipped sensors achieve the measurement accuracy required for the experiment and meet the technical requirements for low-altitude meteorological detection in this study.

To mitigate interference of propeller turbulence on meteorological observations, the airborne meteorological payload was mounted 0.6 m directly above the UAV fuselage. This optimized layout supports continuous, high-frequency in-situ observations of air temperature, atmospheric pressure, relative humidity, atmospheric wind direction and wind speed at a 1 Hz temporal resolution.

2.2 Experimental design and methodology

The experiments were designed with two objectives, each carried out at a separate site. To validate the measurement accuracy of the UAV meteorological sensors, comparative observation experiments were conducted at the Xingtai Field Scientific Experiment Base for Atmospheric Environment, China Meteorological Administration (Figure 2), located in Liulin Town, Neiqiu County, Xingtai City, Hebei Province, China (elevation: 163.6 m). This base is equipped with a 100 m gradient meteorological tower and supporting UAV observation facilities, whose tower-based reference measurements enabled direct accuracy assessment of the UAV sensors. Investigating the impact of atmospheric boundary layer dynamics on UAV flight stability, however, required flights at considerably greater altitudes. Owing to airspace control restrictions at the Xingtai base, these could not be performed there; accordingly, boundary layer flight

https://doi.org/10.5194/egusphere-2026-4218
Preprint. Discussion started: 4 August 2026

disturbance experiments were instead conducted in Qianxian Township, Yuanshi County, where the airspace conditions permitted the higher-altitude flights needed for this part of the study.

The comparative observation experiments were conducted with synchronous measurements from the UAV and the gradient meteorological tower. The UAV operated in two flight modes: vertical ascent/descent and fixed-point hovering at specified heights, with the hovering heights corresponding to the gradient tower levels of 8 m, 16 m, 32 m, 48 m, 64 m, 80 m, and 96 m AGL, respectively. At each corresponding hovering height, a minimum hovering duration of 15 seconds was maintained to ensure sampling stability. And to eliminate mutual observational interference between UAV and gradient tower measurements, the UAV's horizontal flight path was arranged approximately 50 m upwind of the meteorological tower during all field experiments. This spatial layout effectively minimizes the disturbances induced by tower wake flow and UAV rotor downwash on both sets of observational datasets, thereby enabling high-quality simultaneous comparative measurements. The experiments were conducted from July 26th to July 30th, 2025. Each dataset was defined as one complete observation segment comprising a vertical ascent or descent process together with the corresponding fixed-point hovering measurements at each height. On this basis, a total of 39 fixed-point hovering datasets were collected throughout the experimental campaign.

In the boundary layer flight disturbance experiments, the UAV's hovering heights started from 200 m AGL and increased at 200 m intervals up to 1500 m, with a minimum hovering duration of 15 s at each height, consistent with the comparative observation experiments. The experiments were conducted on July 31th, 2025. In addition to conventional meteorological variables, the UAV system continuously synchronously records multi-dimensional data, including flight attitude parameters (pitch angle, roll angle, yaw angle) and real-time flight trajectories. A total of 46 vertical profile datasets were collected throughout the experimental campaign.

2.3 Data processing

For both fixed-point hovering datasets and vertical profile datasets, the same data quality control procedure was applied. Owing to the influence of UAV motion during flight, all non-hovering segments were excluded, and only the data acquired during stable hovering segments

https://doi.org/10.5194/egusphere-2026-4218
Preprint. Discussion started: 4 August 2026

were retained. On this basis, the interquartile range (IQR) method was adopted to identify and remove outliers in meteorological variables, including temperature, atmospheric pressure, relative humidity, wind direction, and wind speed.

To fully exploit the UAV's 1 Hz observations, instead of averaging within each hovering layer before differencing, this study computed pairwise finite differences between every 1 Hz sample of adjacent hovering layers. Let the segment at height z_i contain N_i valid 1 Hz samples of potential temperature ($\theta_{i,m}$) and horizontal wind ($u_{i,m}$, $v_{i,m}$, $m = 1, \ldots, N_i$), and that at z_{i+1} contain N_{i+1} samples ($n = 1, \ldots, N_{i+1}$).

For each sample pair (m, n), the vertical gradients of potential temperature and wind shear were computed as:

$$\left(\frac{\partial \theta}{\partial z}\right)_{m,n} = \frac{\theta_{i+1,n} - \theta_{i,m}}{z_{i+1} - z_i} \tag{1}$$

$$\left(\frac{\partial u}{\partial z}\right)_{m,n} = \frac{u_{i+1,n} - u_{i,m}}{z_{i+1} - z_i} \tag{2}$$

$$\left(\frac{\partial v}{\partial z}\right)_{m,n} = \frac{v_{i+1,n} - v_{i,m}}{z_{i+1} - z_i} \tag{3}$$

Substituting Eqs.1-3 into the definition of the gradient Richardson number equation yileds the following expression for $Ri_{m,n}$:

$$Ri_{m,n} = \frac{g}{\theta_{m,n}} \cdot \frac{\left(\frac{\partial \theta}{\partial z}\right)_{m,n}}{\left(\frac{\partial u}{\partial z}\right)_{m,n}^2 + \left(\frac{\partial v}{\partial z}\right)_{m,n}^2} \tag{4}$$

where $\bar{\theta}_{m,n} = (\theta_{i,m} + \theta_{i+1,n})/2$ is the pair-mean potential temperature and g is the gravitational acceleration. This procedure produces $N_i \times N_{i+1}$ R_i samples for each pair of adjacent hovering measurement layers. The resulting output is a full distribution of Ri values, rather than a single representative value derived from bulk layer-averaged meteorological quantities.

The flight attitude of a UAV responds directly to atmospheric turbulence; therefore, the characteristics of its attitude disturbance can serve as an indirect indicator of turbulence intensity. Accordingly, an attitude turbulence index is constructed from the pitch and roll angular velocities to quantitatively characterize the overall intensity of the UAV flight attitude disturbance induced

https://doi.org/10.5194/egusphere-2026-4218
Preprint. Discussion started: 4 August 2026

by atmospheric turbulence:

$$T = \sqrt{\omega^2 + \phi^2} \tag{5}$$

where ω and ϕ are the pitch angular velocity and roll angular velocity, respectively, and T represents the attitude turbulence index. A higher T value corresponds to stronger atmospheric turbulence and more intense UAV attitude disturbance.

3 Results and discussion

3.1 Analysis of basic meteorological elements from field campaign

To demonstrate the capability of the UAV system in observing the vertical structural characteristics of the near-surface ABL, vertical ascent and descent profile experiments were conducted from July 26 to 30, 2025. These experiments acquired continuous vertical distribution datasets of near-surface meteorological variables, including air temperature, relative humidity, and wind fields. The vertical profile comparisons of meteorological parameters at different heights are summarized in Figure 3.

Overall, the vertical profiles of temperature, relative humidity, wind speed, and wind direction derived from the UAV measurements (red lines) and the gradient tower observations (blue lines) achieve excellent morphological consistency with low statistical errors. Specifically, the wind speed profiles show a negligible bias of 0.02 m/s and an RMSE of 1.11 m/s, while the temperature profiles yield a small bias of 0.10 °C and an RMSE of 0.90 °C, indicating nearly identical profile shapes and minimal systematic deviations between the two observation platforms. Slight fluctuating discrepancies at individual heights are observed for wind direction and relative humidity, with biases of 8.56° and 0.17% and RMSEs of 20.35° and 4.14%, respectively. Despite these minor height-dependent fluctuations, the overall vertical variation trends of the UAV observations align well with the tower benchmark data, and all deviations remain within a reasonable and acceptable range. These results verify that the UAV-borne meteorological payload can accurately capture the vertical distribution patterns of ABL meteorological variables and maintain stable observational precision across all detected heights, demonstrating that the UAV platform fully meets the technical requirements for refined vertical profile detection of low-altitude atmospheric environments.

https://doi.org/10.5194/egusphere-2026-4218
Preprint. Discussion started: 4 August 2026

Synchronized observations from the UAV and the gradient meteorological tower were further adopted to compare and validate the vertical profiles of key thermodynamic and dynamic parameters within the ABL, with the comparative results illustrated in Figure 4. The vertical profiles of potential temperature (θ) and gradient Richardson number (Ri) derived from the UAV measurements achieve favorable consistency with the tower observations. For potential temperature, the CC reaches 0.64, with a bias of 0.15 K and an RMSE of 0.85 K; its vertical profile morphology and gradient characteristics are in good agreement with the tower benchmark data, demonstrating that the UAV system can accurately resolve the vertical thermal stratification structure of the ABL. For the gradient Ri, the CC is likewise 0.64, accompanied by an extremely low bias of −0.01 and an RMSE of 0.05, indicating that the UAV reliably identifies the dynamic stability regimes at all vertical layers of the ABL without noticeable altitude-dependent systematic deviations. These findings indicate that the UAV-borne meteorological system is capable of not only directly acquiring high-quality profiles of conventional meteorological variables but also accurately retrieving key thermodynamic and dynamic parameters of the boundary layer, further validating that the multi-rotor UAV platform is well suited for refined observational characterization and stability mechanism analysis of low-altitude atmospheric processes.

3.2 Impacts of ABL Spatiotemporal Evolution on UAV Flight Attitude

Three typical UAV low-level sounding campaigns, conducted during three successive periods (18:24–18:43, 18:55–19:22, and 19:43–19:55 BJT) on the evening of July 31, 2025 in Qianxian Township, Yuanshi County, Hebei Province, were selected for representative case analysis. The study area is located in the hilly transitional zone on the eastern piedmont of the Taihang Mountains, featuring a typical mountain–plain transition terrain dominated by alternating hills and low mountains. The local weather condition shifted from cloudy to overcast on the afternoon of July 31. Analysis of hourly ECMWF ERA5 pressure-level synoptic fields (Figure 5a) shows that a shallow upper-level trough moved eastward. Below 850 hPa, the region was dominated by southerly winds and weak moisture advection, accompanied by weak easterly wind convergence at 925 hPa, with low-level relative humidity ranging from 60% to 80%. Under this synoptic background, sporadic light drizzle occurred in Qianxian Township from 18:00 to

https://doi.org/10.5194/egusphere-2026-4218
Preprint. Discussion started: 4 August 2026

20:00 BJT.

Time–height cross sections of low-level vertical wind shear (Figure 5c) indicate that the observation window corresponded to a transition stage during which the convective atmospheric boundary layer (CABL) gradually evolved into a stable atmospheric boundary layer (SABL). The wind shear field exhibited distinct layered structures and evident temporal evolutionary characteristics. In the near-surface layer (60–200 m AGL), jointly modulated by diurnal ABL evolution and topographic forcing, steady positive vertical wind shear persisted and increased with height (red shaded areas), with shear magnitudes predominantly ranging from 0 to 3×10^{-3} s^{-1}. This phenomenon is closely associated with evening surface radiative cooling and weakened turbulent mixing. By contrast, the middle and upper layers (200–1500 m AGL) presented fluctuating vertical structures characterized by alternating positive and negative wind shear zones. Notably, prominent negative shear regimes occurred at 200–800 m AGL during 17:45–18:30 and 19:15–20:00 BJT (blue shaded areas), with maximum shear intensities reaching 3×10^{-3} s^{-1}. The three UAV sounding trajectories (ascent and descent segments denoted by solid/dashed black, red, and blue lines, respectively) fully captured this critical ABL transition process.

(1) Case of UAV sounding Experiment from 18:24 to 18:43

Combined with the vertical structure of atmospheric physical environmental fields (Figure 6) and UAV attitude response profiles (Figure 7), the near-surface stable ABL (200–400 m AGL) is characterized by a rapid increase in potential temperature with height, forming a strongly stable stratification regime with Richardson number (Ri) greater than 0.25, where turbulent motions are substantially suppressed. In this layer, wind speed increases gently with height, generating weak vertical wind shear. Under the coupled constraints of strong thermal stability and insignificant dynamic shear, the deviations of UAV pitch and roll angles are both limited within ±1°, the fluctuation range of attitude angular velocity is lower than 0.05 °/s, and the turbulence index remains below 5, corresponding to generally stable UAV flight attitudes.

In the weakly stratified middle-upper layer (400–1000 m AGL), the potential temperature gradient decreases significantly, and the atmospheric stratification approaches a neutral state, with Ri fluctuating between 0 and 0.25, which provides favorable conditions for turbulent development. Meanwhile, wind speed rises sharply with height, producing intense vertical wind shear. In this layer, UAV pitch and roll angles exhibit distinct oscillatory disturbances; the

https://doi.org/10.5194/egusphere-2026-4218
Preprint. Discussion started: 4 August 2026

fluctuation amplitude of attitude angular velocity expands to ±0.15 °/s, and the turbulence index peaks at 8–15. This layer dominates the most prominent attitude perturbations and flight bumpiness throughout the entire radiosounding process.

The upper strongly stable layer (1000–1400 m AGL) features a re-intensified potential temperature gradient, with *Ri* rebounding above 0.25. The atmospheric stratification returns to a highly stable state that effectively inhibits turbulent activities. Wind speed decreases slightly with height, accompanied by weakened vertical shear. Restricted by the combined effects of restored thermal stability and weakened dynamic shear, the fluctuations of UAV attitude angular velocity gradually decay, the turbulence index declines steadily, and flight stability recovers, presenting consistent response characteristics with the near-surface stable layer.

Furthermore, the relative humidity profile reveals a persistent high-humidity zone (RH > 80%) at 200–400 m AGL during the UAV descent phase. However, this moist layer corresponds to weak turbulent activity and stable flight attitudes, demonstrating that water vapor concentration alone is not a dominant factor inducing UAV attitude disturbances. During the descent process, local cloud clusters shift southeastward, increasing low-level atmospheric moisture content and reducing ambient wind speed, which slightly enhances local atmospheric instability within the low-level and in-cloud layers. In contrast, the middle and upper layers are predominantly dry and cloud-free, eliminating additional interference from cloud droplet impacts and in-cloud buoyancy perturbations. These observational phenomena further confirm that UAV attitude disturbances in complex terrain are primarily governed by dynamic turbulence modulated by the synergistic effects of vertical wind shear and atmospheric stratification stability, rather than moisture conditions..

(2) Case of UAV Radiosounding Experiment from 18:55 to 19:22

The thermal, dynamic, and humidity variables of the ABL exhibited pronounced vertically stratified evolutionary characteristics during the observation period (Figure 8), with the corresponding UAV attitude responses shown in Figure 9.. In the near-surface layer of 200~600 m AGL, the *Ri* consistently exceeded 0.25, corresponding to strongly stable atmospheric stratification, weak vertical wind shear, and substantially suppressed turbulent motion, thereby forming an overall quiescent low-altitude atmospheric environment.

In the middle layer of 600~1000 m AGL, the vertical gradient of potential temperature

https://doi.org/10.5194/egusphere-2026-4218
Preprint. Discussion started: 4 August 2026

weakened markedly, and the atmospheric stratification gradually approached a neutral state. Meanwhile, the vertical wind speed gradient increased sharply, providing favorable dynamical conditions for the development of flow instability. Additionally, the vertical moisture distribution presented notable discrepancies between UAV ascent and descent observations

The upper layer of 1000~1400 m AGL near the cloud base was characterized by weakly unstable stratification and the maximum vertical wind shear throughout the profile. Enhanced entrainment processes promoted vigorous turbulent development, substantially facilitating momentum and water vapor exchange between upper and lower atmospheric layers. Accordingly, atmospheric disturbance intensity increased steadily with altitude in this zone.

In the stably stratified near-surface layer with low turbulence levels, the RMSE fluctuation amplitudes of UAV pitch and roll angles were all below 1.8°, the mean dynamic attitude angular velocity remained within 0.3° •s^{-1}, and the vertical acceleration fluctuations were confined within ±0.10 m • s^{-2}. These quantitative metrics further verify that strong static stability effectively suppresses local airflow pulsations. And at high altitudes near the cloud base with intense dynamic disturbances, UAV attitude perturbations reached their maximum magnitudes across the entire vertical profile. Specifically, the RMSE attitude angle fluctuation exceeded 3.9°, the instantaneous peak angular velocity reached 0.82° • s^{-1}, and the extreme vertical acceleration fluctuations surpassed ±0.30 m·s^{-2}. The superposition of intensive local turbulence and compound vertical wind shear ultimately triggered severe in-flight bumpiness and prominent attitude oscillations.

The combined effects of downdraft convergence beneath the cloud base, spatial heterogeneity of local flow fields, and divergent dynamic environments along ascent and descent trajectories generated distinctly asymmetric evolutionary patterns in UAV dynamic attitude responses during outbound and return flights. These findings demonstrate that vertical stratification differences in atmospheric thermal structures and dynamic flow fields are the dominant factors driving the spatiotemporal heterogeneity of multi-rotor UAV flight attitude disturbances over complex terrain.

(3) A case of UAV sounding experiment from 19:43 to 19:55

The atmospheric thermal and dynamic structures over the study area exhibited remarkable

https://doi.org/10.5194/egusphere-2026-4218
Preprint. Discussion started: 4 August 2026

vertical stratification and spatial inhomogeneity (Figure 10). In terms of thermal characteristics, potential temperature generally increased with height under predominantly stable stratification, with distinct differences observed between in-cloud and out-of-cloud layers (approximately 900~1200 m). A steeper vertical gradient of potential temperature occurred when the UAV penetrated the cloud layer, indicating substantially enhanced static stability within the cloud. Relative humidity profiles differed considerably between ascent and descent phases, notably lower low-level humidity during descent revealed prominent horizontal inhomogeneity in moisture distributions across cloudy and clear-sky regions. Dynamically, the wind field was dominated by intense vertical shear, with wind speed generally increasing with height and wind shear drastically amplified near the cloud layer. In the lower layer (200~800 m), the *Ri* approached zero, representing dynamically unstable conditions that favored turbulent generation and development. Above the cloud layer, *Ri* increased sharply, restoring atmospheric stability and suppressing turbulent activities. Such vertical disparities in thermal stratification and dynamic stability constituted the dominant atmospheric background modulating UAV flight states. Quantitative correlations between spatiotemporal variations in atmospheric thermodynamic conditions and UAV flight attitude parameters are illustrated in Figure 11, which reveals significant layered differences in the perturbation magnitudes of attitude angles, turbulence indices, and vertical motion between UAV ascent and descent processes.

In terms of attitude angle variations, the UAV pitch angle remained consistently positive at 2–6° during ascent, declining gently with altitude with a small standard deviation and smooth flight performance. Correspondingly, the roll angle stabilized near 0° , with overall deviations constrained within ±1°. In contrast, the pitch angle was predominantly negative (−5~−1°) throughout the descent phase. Dramatically amplified angle fluctuations were observed within the dynamically unstable 200–800 m layer, where the standard deviation of pitch angle nearly doubled relative to the ascent phase. Meanwhile, the roll angle exhibited substantial negative offsets exceeding −3°. These distinct discrepancies demonstrate that crosswind disturbances and lift fluctuations induced by spatially heterogeneous low-level wind and thermal conditions significantly distort the UAV airframe attitude during descent.

With respect to turbulence intensity and vertical motion metrics, the dynamically unstable

https://doi.org/10.5194/egusphere-2026-4218
Preprint. Discussion started: 4 August 2026

200~800 m layer exhibited a markedly higher turbulence index during descent than during ascent, with the maximum turbulence magnitude occurring near the surface. By comparison, the ascent phase maintained low turbulence levels and weak fluctuations across this layer. Driven by ambient turbulent pulsations, high-frequency oscillations of vertical acceleration were detected at low altitudes during both flight phases. The peak-to-trough difference in vertical acceleration exceeded 0.15 $m \cdot s^{-2}$ during ascent, indicative of intense local aerodynamic perturbations. In the stable cloud-top layer above 1000 m, enhanced atmospheric dynamic stability effectively suppressed turbulent activities, restricting vertical acceleration fluctuations within ±0.03 $m \cdot s^{-2}$ and restoring all attitude parameters to a stable state.

Collectively, the quantitative observational results confirm a strong negative correlation between atmospheric dynamic stability and the fluctuation amplitude of UAV flight parameters. Intense low-level turbulence and vertically heterogeneous thermal-dynamic atmospheric structures are identified as the primary drivers of asymmetric attitude disturbances and divergent unsteady flight performance between UAV ascent and descent trajectories over complex terrain.

3.3 Vertical wind shear and Ri *impacts on UAV attitude in flight disturbance experiments*

The joint distribution of the Ri and vertical wind shear (Figure 12) illustrates how atmospheric stratification stability and dynamic forcing jointly modulate turbulence intensity, thereby governing UAV flight attitude disturbances. The number within each grid cell denotes the sample count, the cell color indicates the mean turbulence index (TI), and the top and right marginal distributions present the mean TI averaged along the Ri and wind-shear directions, respectively. Vertical wind shear, the primary dynamic source of mechanical turbulence, couples with Ri—which quantifies stratification stability—to jointly control boundary-layer turbulence.

The observations are predominantly concentrated within vertical wind shear of approximately 0.005–0.020 s^{-1} and Ri between −1 and 3, narrowing toward Ri ≈ 0–1 as wind shear increases and forming a triangular distribution. This indicates that strong wind shear tends to co-occur with near-neutral stratification, whereas large shear combined with strongly stable stratification is rare.

Overall, the TI tends to increase with vertical wind shear, consistent with the expectation

https://doi.org/10.5194/egusphere-2026-4218
Preprint. Discussion started: 4 August 2026

that stronger dynamic shear intensifies mechanical turbulence and aggravates flight bumpiness. Under unstable stratification (Ri < 0), the mean TI is further elevated (exceeding 2.9 in the top marginal distribution), as thermal convection superimposed on shear-induced disturbances enhances turbulence, readily triggering pronounced pitch, roll, and yaw oscillations and increasing the flight control burden.

Notably, a localized zone of anomalously high TI (approaching or exceeding 3.0) appears at moderate wind shear (approximately 0.007–0.010 s^{-1}) combined with near-zero to negative Ri, deviating from the general monotonic trend. This may not stem from atmospheric forcing alone. One plausible explanation is that, within this range, the characteristic scale of turbulent eddies may become comparable to the airframe dimensions and approach the intrinsic dynamic response frequency of the multi-rotor UAV, potentially inducing a resonance-like amplification of the attitude response beyond what the ambient turbulence intensity alone would suggest. This interpretation remains tentative and warrants further verification through controlled experiments and platform-specific dynamic response analysis.

Within the near-neutral to weakly stable regime , samples are most densely populated, forming a high-frequency turbulence zone where stratification only weakly inhibits turbulent development, so that even moderate wind shear can excite noticeable perturbations and minor attitude oscillations. As stratification transitions toward the strongly stable regime , thermal suppression intensifies and partially counteracts shear-induced disturbances, corresponding to relatively stable flight states.

In summary, the coupling of vertical wind shear and stratification stability jointly shapes ABL turbulence, with flight bumpiness generally intensifying as wind shear strengthens. Beyond this atmospheric forcing, the potential coupling between turbulence scales and the UAV's own dynamic characteristics may further modulate the attitude response in certain regimes. Together, these factors dominate UAV attitude disturbances and fundamentally determine the flight stability of low-altitude UAV observations over complex terrain.

4 Concluding remarks

This study investigated the measurement performance and the environment–platform coupling of a multi-rotor UAV (DJI Matrice 350 RTK) for atmospheric boundary layer (ABL)

https://doi.org/10.5194/egusphere-2026-4218
Preprint. Discussion started: 4 August 2026

observation over complex terrain, based on co-located comparison experiments at the Xingtai Field Scientific Experiment Base and boundary layer flight disturbance experiments in Qianxian Township, Yuanshi County, Hebei Province. Two objectives were addressed: validating the accuracy of UAV-derived meteorological and stability parameters against a gradient meteorological tower and clarifying how vertical wind shear and stratification stability jointly modulate UAV attitude disturbances.

The accuracy validation demonstrates that the UAV-borne meteorological payload can reliably capture the vertical structure of the near-surface ABL. Compared with the 100 m gradient tower, the UAV measurements achieved excellent morphological consistency and low statistical errors across all detected heights, with negligible biases in wind speed (0.02 m/s) and temperature (0.10 °C), and acceptable deviations in wind direction and relative humidity. Importantly, the UAV also accurately retrieved derived thermodynamic and dynamic parameters, including potential temperature (CC = 0.64, RMSE = 0.85 K) and the gradient Richardson number (CC = 0.64, RMSE = 0.05), confirming that the platform resolves not only conventional variables but also the thermal stratification and dynamic stability regimes of the boundary layer.

The attitude-response analysis reveals that UAV flight disturbances over complex terrain are primarily governed by dynamic turbulence generated through the coupling of vertical wind shear and stratification stability, rather than by moisture conditions. Across three representative sounding cases spanning the transition from a convective to a stable boundary layer, attitude disturbances (pitch, roll, angular velocity, and the turbulence index T) were suppressed in strongly stable layers ($Ri > 0.25$) and amplified in near-neutral or weakly unstable layers ($0 < Ri < 0.25$ or $Ri < 0$) where intense wind shear coincided with weak thermal suppression. Pronounced asymmetries between ascent and descent trajectories further indicate that spatially heterogeneous low-level flow and thermal structures drive the spatiotemporal heterogeneity of flight disturbances.

The joint distribution of Ri and vertical wind shear shows that turbulence intensity, and hence flight bumpiness, generally intensifies as wind shear strengthens, with the strongest disturbances under unstable stratification, while strongly stable stratification ($Ri > 2$–3) partially counteracts shear-induced disturbances. A localized anomaly of elevated turbulence response at moderate shear and near-zero to negative Ri suggests a possible resonance-like coupling between

https://doi.org/10.5194/egusphere-2026-4218
Preprint. Discussion started: 4 August 2026

turbulent eddy scales and the UAV's own dynamic response, though this interpretation remains tentative and requires further study. Overall, these findings establish quantitative thresholds relevant to both reliable UAV-based ABL sensing and safe low-altitude flight-safety assessment, supporting the use of multi-rotor UAVs as a valuable intermediate observing platform for refined boundary-layer characterization over station-sparse, complex-terrain regions.

Data availability

All observational data used in this study, comprising the 1-min gradient meteorological tower records for July 2025 and the 1-Hz UAV-borne sonde measurements are accessible from Yang, R (2026).

Author contribution

Conceptualization: JianpingGuo, RongfangYang

Datacuration: RongfangYang

Formalanalysis: DeliMeng, ZhenZhang, RongfangYang

Fundingacquisition: RongfangYang

Investigation: RongfangYang, DeliMeng, ZhenZhang, JianpingGuo

Methodology: RongfangYang, DeliMeng, Lihui Liu, Guocui Li, Guanglei Zhang

Projectadministration: RongfangYang

Resources: Jianping Guo, RongfangYang, DeliMeng

Software: Zhen Zhang, RongfangYang, Lihui Liu, Guocui Li

Supervision: Jianping Guo

Validation: RongfangYang, Zhen Zhang, Jianping Guo, DeliMeng

Visualization: RongfangYang, DeliMeng, Guanglei Zhang

Writing– original draft: RongfangYang,Zhen Zhang, DeliMeng, Jianping Guo, Lihui Liu, Guocui Li

Writing– review & editing: Zhen Zhang, RongfangYang, Jianping Guo, DeliMeng

Competing interests

The authors declare no conflicts of interest relevant to this study.

Acknowledgments

The authors would like to acknowledge the Xingtai Neiqiu Field Scientific Experiment Base for the observational support and experimental facilities provided for this study. This research has been supported by the project "Research on Key Technologies for Monitoring and Nowcasting of Low-Altitude Hazardous Weather over Complex Underlying Surfaces in the Beijing-Tianjin-Hebei Region" (grant no. CXFZ2025J107).

References

Barbieri, L., Kral, S. T., Bailey, S. C. C., Frazier, A. E., Jacob, J. D., Reuder, J., Brus, D., Chilson, P. B., Crick, C., Detweiler, C., Doddi, A., Elston, J., Foroutan, H., González-Rocha, J., Greene, B. R., Guzman, M. I., Houston, A. L., Islam, A., Kemppinen, O., … de Boer, G.: Intercomparison of small unmanned aircraft system (sUAS) measurements for atmospheric science during the LAPSE-RATE campaign, Sensors, 19, 2179, https://doi.org/10.3390/s19092179, 2019.

Cassano, J. J.: Observations of atmospheric boundary layer temperature profiles with a small unmanned aerial vehicle, Antarct. Sci., 26, 205–213, https://doi.org/10.1017/S0954102013000539, 2014.

Chang, C.-C., Chang, C.-Y., Wang, J.-L., Pan, X.-X., Chen, Y.-C., and Ho, Y.-J.: An optimized multicopter UAV sounding technique (MUST) for probing comprehensive atmospheric variables, Chemosphere, 254, 126867, https://doi.org/10.1016/j.chemosphere.2020.126867, 2020.

Garratt, J. R.: The Atmospheric Boundary Layer, Cambridge University Press, Cambridge, UK, 1992.

Groos, A. R., Brand, N., Bronz, M., and Philipp, A.: Atmospheric sounding of the boundary layer over alpine glaciers using fixed-wing UAVs, Atmos. Meas. Tech., 18, 6493–6512, https://doi.org/10.5194/amt-18-6493-2025, 2025.

Hansche, I., Shahi, S., Abermann, J., and Schöner, W.: The vertical atmospheric structure of the partially glacierised Mittivakkat valley, southeast Greenland, J. Glaciol., 69, 1097–1108, https://doi.org/10.1017/jog.2022.120, 2023.

Hobbs, S., Dyer, D., Courault, D., Olioso, A., Lagouarde, J.-P., Kerr, Y., McAneney, J., and Bonnefond, J.-M.: Surface layer profiles of air temperature and humidity measured from

https://doi.org/10.5194/egusphere-2026-4218
Preprint. Discussion started: 4 August 2026

unmanned aircraft, Agronomie, 22, 635–640, https://doi.org/10.1051/agro:2002050, 2002.

Illingworth, A. J., Cimini, D., Haefele, A., Haeffelin, M., Hervo, M., Kotthaus, S., Löhnert, U., Martinet, P., Mattis, I., O'Connor, E. J., and Potthast, R.: How can existing ground-based profiling instruments improve European weather forecasts?, Bull. Am. Meteorol. Soc., 100, 605–619, https://doi.org/10.1175/BAMS-D-17-0231.1, 2019.

Jonassen, M. O., Tisler, P., Altstädter, B., Scholtz, A., Vihma, T., Lampert, A., König-Langlo, G., and Lüpkes, C.: Application of remotely piloted aircraft systems in observing the atmospheric boundary layer over Antarctic sea ice in winter, Polar Res., 34, 25651, https://doi.org/10.3402/polar.v34.25651, 2015.

Li, S., Xing, M., Jiang, L., Chen, P., Ding, F., and Yang, W.: Vertical variation of atmospheric particulate matter under different pollution levels in the suburbs of Tianjin based on unmanned aerial vehicle, J. Air Waste Manage. Assoc., 72, 1463–1476, https://doi.org/10.1080/10962247.2022.2134231, 2022.

Mamali, D., Marinou, E., Sciare, J., Pikridas, M., Kokkalis, P., Kottas, M., Binietoglou, I., Tsekeri, A., Keleshis, C., Engelmann, R., Baars, H., Ansmann, A., Amiridis, V., Russchenberg, H., and Biskos, G.: Vertical profiles of aerosol mass concentration derived by unmanned airborne in situ and remote sensing instruments during dust events, Atmos. Meas. Tech., 11, 2897–2910, https://doi.org/10.5194/amt-11-2897-2018, 2018.

Palomaki, R. T., Rose, N. T., van den Bossche, M., Sherman, T. J., and De Wekker, S. F. J.: Wind estimation in the lower atmosphere using multirotor aircraft, J. Atmos. Ocean. Technol., 34, 1183–1191, https://doi.org/10.1175/JTECH-D-16-0177.1, 2017.

Pusfitasari, E. D., Ruiz-Jimenez, J., Tiusanen, A., Suuronen, M., Haataja, J., Wu, Y., Kangasluoma, J., Luoma, K., Petäjä, T., Jussila, M., Hartonen, K., and Riekkola, M.-L.: Vertical profiles of volatile organic compounds and fine particles in atmospheric air by using an aerial drone with miniaturized samplers and portable devices, Atmos. Chem. Phys., 23, 5885–5904, https://doi.org/10.5194/acp-23-5885-2023, 2023.

Reuder, J., Jonassen, M. O., and Ólafsson, H.: The Small Unmanned Meteorological Observer SUMO: recent developments and applications of a micro-UAS for atmospheric boundary layer research, Acta Geophys., 60, 1454–1473, https://doi.org/10.2478/s11600-012-0042-8, 2012.

https://doi.org/10.5194/egusphere-2026-4218
Preprint. Discussion started: 4 August 2026

Seibert, P., Beyrich, F., Gryning, S.-E., Joffre, S., Rasmussen, A., and Tercier, P.: Review and intercomparison of operational methods for the determination of the mixing height, Atmos. Environ., 34, 1001–1027, https://doi.org/10.1016/S1352-2310(99)00349-0, 2000.

Shelekhov, A., Afanasiev, A., Shelekhova, E., Kobzev, A., Tel'minov, A., Molchunov, A., and Poplevina, O.: Low-altitude sensing of urban atmospheric turbulence with UAV, Drones, 6, 61, https://doi.org/10.3390/drones6030061, 2022.

Shimura, T., Inoue, M., Tsujimoto, H., Sasaki, K., and Iguchi, M.: Estimation of wind vector profile using a hexarotor unmanned aerial vehicle and its application to meteorological observation up to 1000 m above surface, J. Atmos. Ocean. Technol., 35, 1621 – 1631, https://doi.org/10.1175/JTECH-D-17-0186.1, 2018.

Stith, J. L., Baumgardner, D., Haggerty, J., Hardesty, R. M., Lee, W.-C., Lenschow, D., Pilewskie, P., Smith, P. L., Steiner, M., and Vömel, H.: 100 years of progress in atmospheric observing systems, Meteorol. Monogr., 59, 2.1–2.55, https://doi.org/10.1175/AMSMONOGRAPHS-D-18-0006.1, 2018.

Stull, R. B.: An Introduction to Boundary Layer Meteorology, Kluwer Academic Publishers, Dordrecht, the Netherlands, 1988.

Wang, B. H., Wang, D. B., Ali, Z. A., Ting, B. T., and Wang, H.: An overview of various kinds of wind effects on unmanned aerial vehicle, Meas. Control, 52, 731–739, https://doi.org/10.1177/0020294019847688, 2019.

Wang, J.-Y., Luo, B., Zeng, M., and Meng, Q.-H.: A wind estimation method with an unmanned rotorcraft for environmental monitoring tasks, Sensors, 18, 4504, https://doi.org/10.3390/s18124504, 2018.

Weber, K., Heweling, G., Fischer, C., and Lange, M.: The use of an octocopter UAV for the determination of air pollutants – a case study of the traffic induced pollution plume around a river bridge in Duesseldorf, Germany, Int. J. Environ. Sci., 2, 63–68, 2017.

Wetz, T., Wildmann, N., and Beyrich, F.: Distributed wind measurements with multiple quadrotor unmanned aerial vehicles in the atmospheric boundary layer, Atmos. Meas. Tech., 14, 3795–3814, https://doi.org/10.5194/amt-14-3795-2021, 2021.

Wulfmeyer, V., Hardesty, R. M., Turner, D. D., Behrendt, A., Cadeddu, M. P., Di Girolamo, P., Schlüssel, P., Van Baelen, J., and Zus, F.: A review of the remote sensing of lower

https://doi.org/10.5194/egusphere-2026-4218
Preprint. Discussion started: 4 August 2026

tropospheric thermodynamic profiles and its indispensable role for the understanding and the simulation of water and energy cycles, Rev. Geophys., 53, 819–895, https://doi.org/10.1002/2014RG000476, 2015.

Yang, R.: Multi-rotor UAV and gradient tower observations of the atmospheric boundary layer over the eastern Taihang piedmont, Hebei, China (July 2025), Zenodo [data set], https://doi.org/10.5281/zenodo.21356413, 2026.

Zhou, Y., Qiao, C., Zhou, M., Wang, Y., Tian, X., Wang, Y., and Duan, M.: Observation of greenhouse gas vertical profiles in the boundary layer of the Mount Qomolangma region using a multirotor UAV, Atmos. Meas. Tech., 18, 1609–1619, https://doi.org/10.5194/amt-18-1609-2025, 2025.

https://doi.org/10.5194/egusphere-2026-4218
Preprint. Discussion started: 4 August 2026

Figures

Figure 1. (a) Snap shot of the meteorological tower deployed at the Xingtai Field Scientific Experiment Base; (b) The multi-rotor UAV platform and integrated airborne meteorological payload used for field observations in this study.

https://doi.org/10.5194/egusphere-2026-4218
Preprint. Discussion started: 4 August 2026

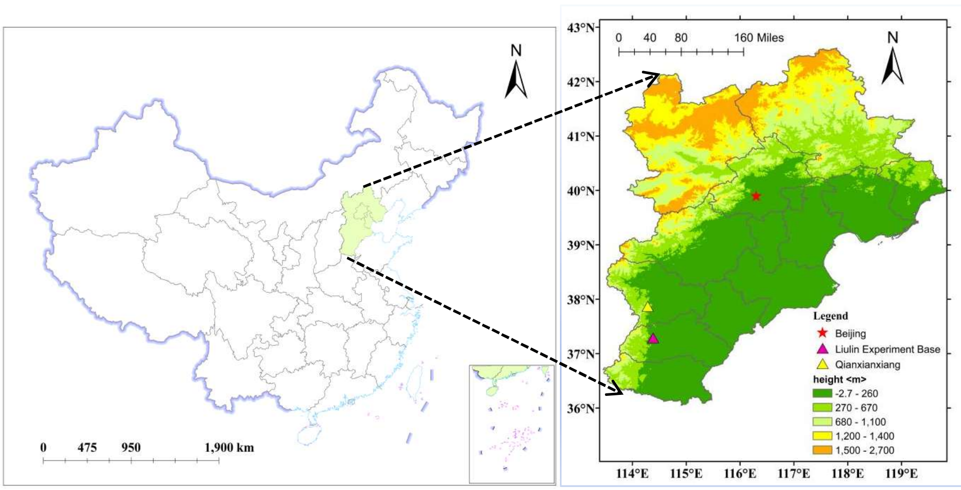

Figure 2. Topographical map of the surrounding area of the Aerodinamic Environment Field Scientific Experiment Base, showing the location of the gradient meteorological tower (red triangle).

https://doi.org/10.5194/egusphere-2026-4218
Preprint. Discussion started: 4 August 2026

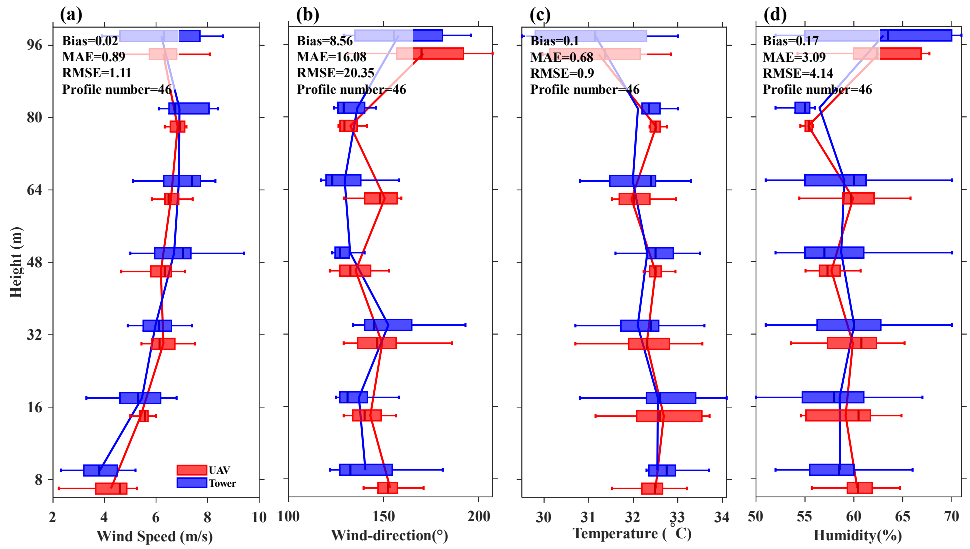

Figure 3. Vertical profiles of meteorological elements observed by the UAV platform and gradient meteorological tower during the period from July 26 to 30, 2025: (a) wind speed, (b) wind direction, (c) air temperature, (d) relative humidity.

https://doi.org/10.5194/egusphere-2026-4218
Preprint. Discussion started: 4 August 2026

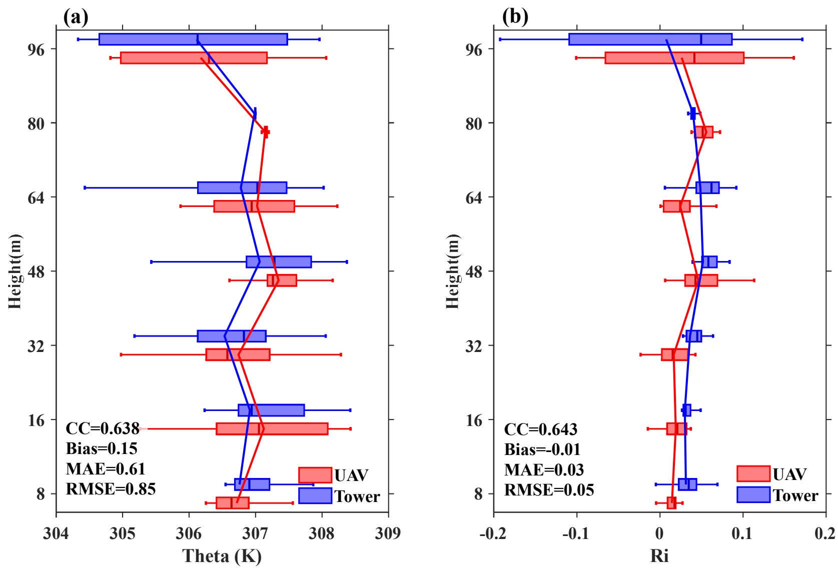

Figure 4. Vertical profiles of key atmospheric parameters observed by the UAV platform and gradient meteorological tower during the period from July 26 to 30, 2025: (a) potential temperature (θ), (b) gradient Richardson number (Ri)

https://doi.org/10.5194/egusphere-2026-4218
Preprint. Discussion started: 4 August 2026

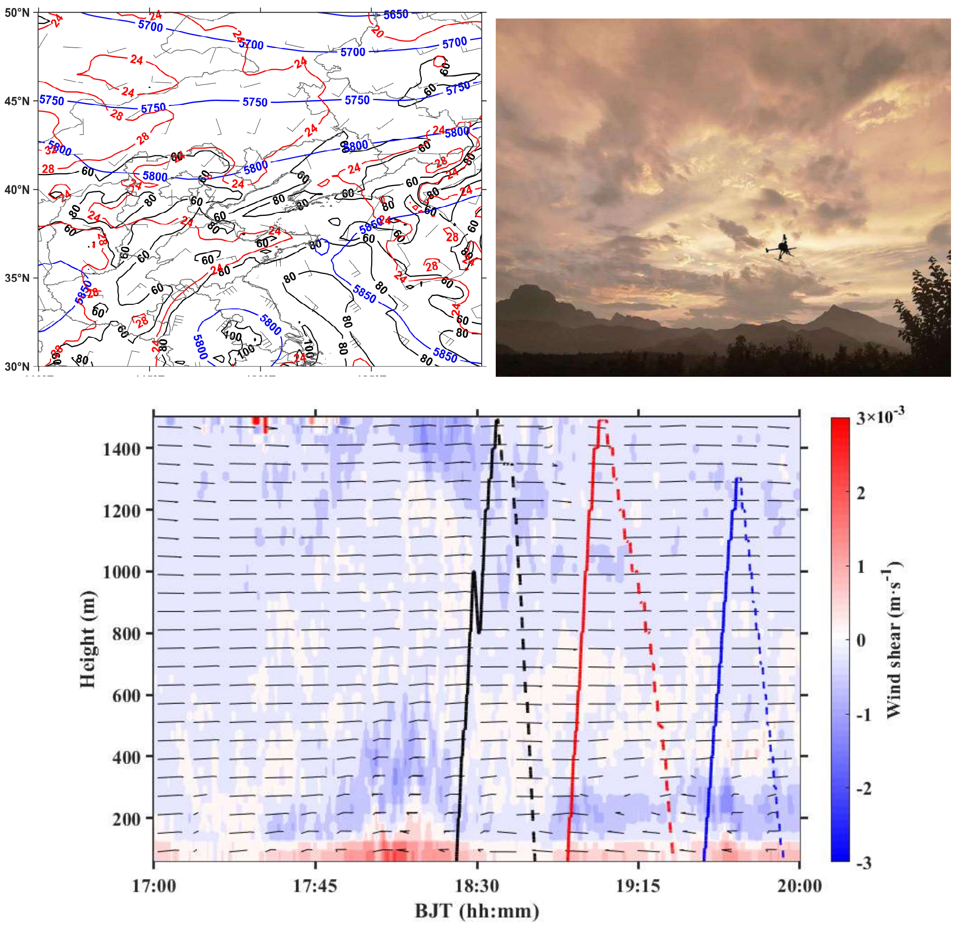

Figure 5. (a) Spatial distributions of the 500 hPa geopotential height (blue contours, units: gpm), 925 hPa temperature (red contours, units: °C), 925 hPa relative humidity (black contours, units: %), and horizontal wind field (wind barbs) at 14:00 BJT on July 31, 2025. (b) Vertical profiles derived from UAV hovering observations at Qianxian Township on July 31, 2025. (c) Time-height cross section of the wind field from 17:00 to 20:00 BJT on July 31, 2025. The shaded contours represent the magnitude of vertical wind shear of horizontal winds; positive values indicate normal shear (wind speed increases with height), while negative values denote reverse shear (wind speed decreases with height, units: s^{-1}). The solid and dashed black, red, and blue lines represent the ascent and descent trajectories of the three UAV sounding flights, respectively: black for 18:24~18:43 BJT, red for 18:55~19:22 BJT, and blue for 19:43~19:55 BJT.

https://doi.org/10.5194/egusphere-2026-4218
Preprint. Discussion started: 4 August 2026

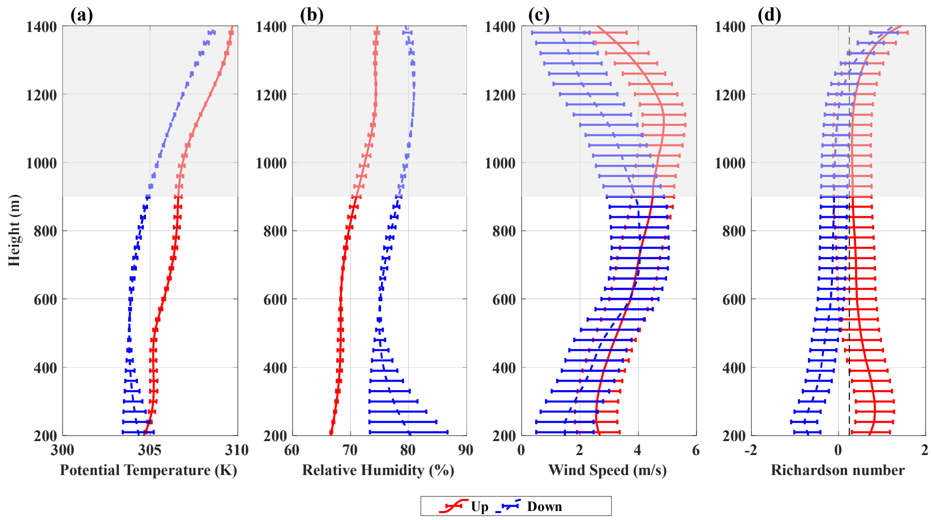

Figure 6. Vertical profiles of atmospheric background field during 18:24–18:43 BJT on July 31, 2025: (a) potential temperature, (b) relative humidity, (c) wind speed, (d) gradient Richardson number

https://doi.org/10.5194/egusphere-2026-4218
Preprint. Discussion started: 4 August 2026

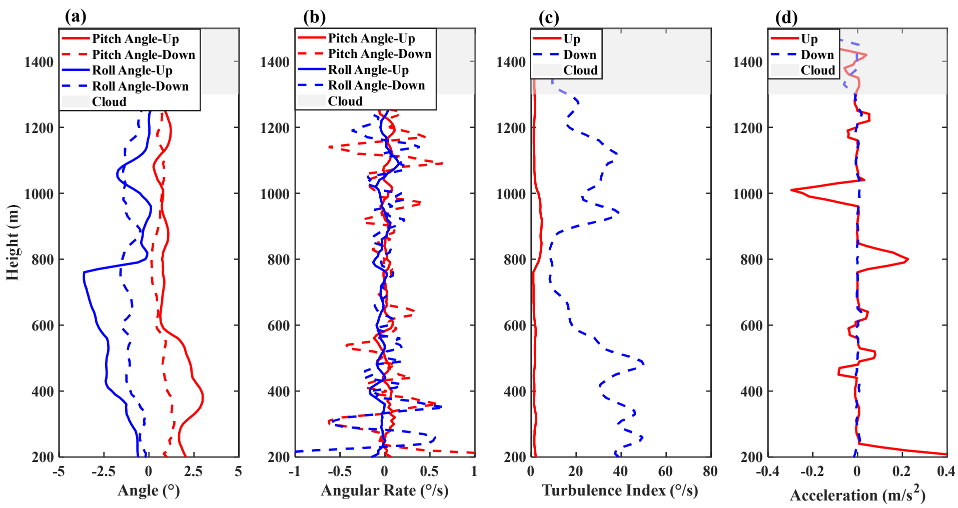

Figure 7. Vertical response profiles of UAV flight attitude parameters during 18:24–18:43 on July 31, 2025: (a) attitude angles profile, (b) angular rate profile, (c) turbulence index profile, (d) vertical acceleration profile

https://doi.org/10.5194/egusphere-2026-4218
Preprint. Discussion started: 4 August 2026

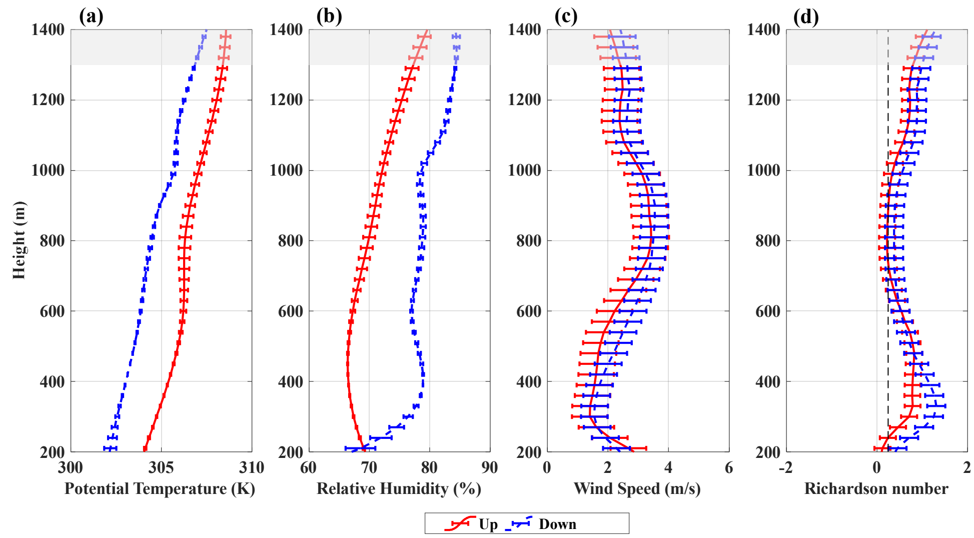

Figure 8. Same as Figure 6, but for the period of 18:55–19:22 BJT on July 31, 2025.

https://doi.org/10.5194/egusphere-2026-4218
Preprint. Discussion started: 4 August 2026

702 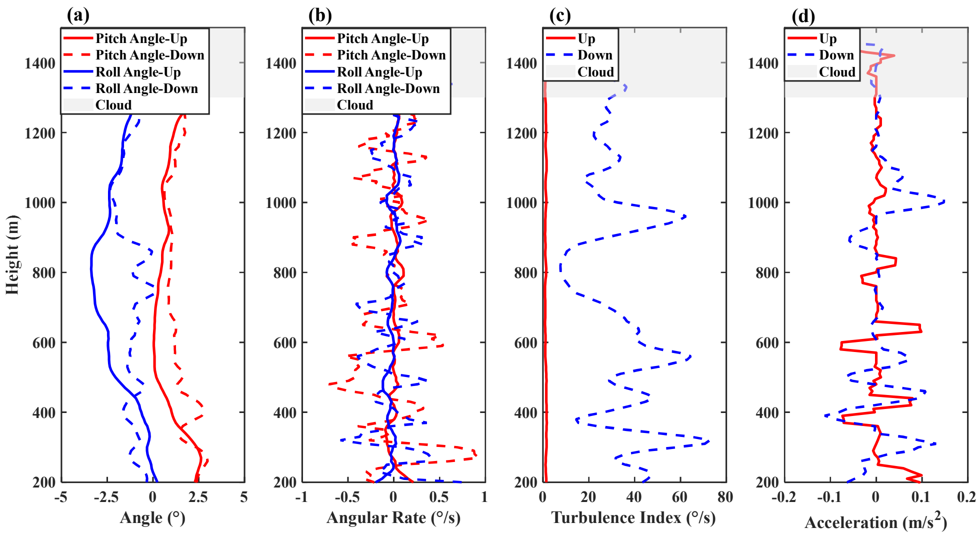

703 **Figure 9.** Same as Figure 7, but for the period of 18:55–19:22 BJT on July 31, 2025.

704

https://doi.org/10.5194/egusphere-2026-4218
Preprint. Discussion started: 4 August 2026

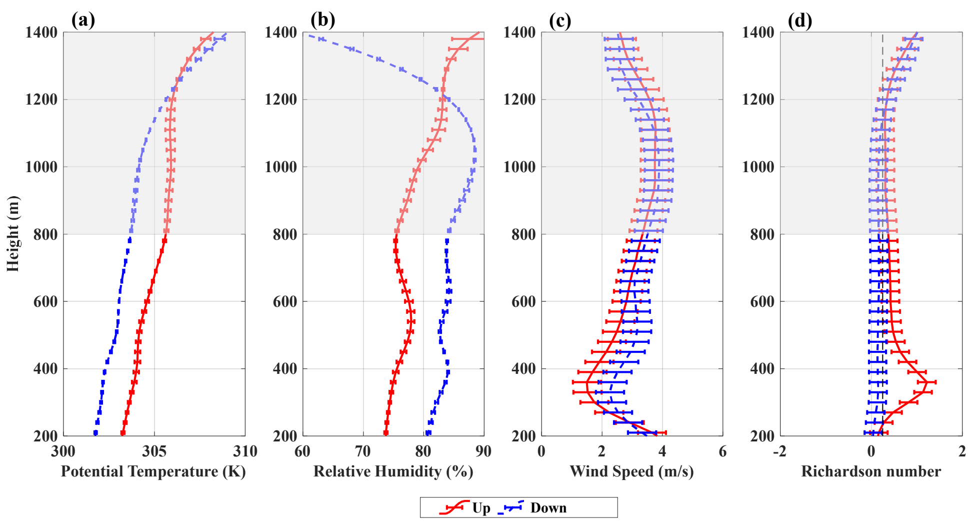

Figure 10. Same as Figure 8, but for the period of 19:43–19:55 BJT on July 31, 2025.

https://doi.org/10.5194/egusphere-2026-4218
Preprint. Discussion started: 4 August 2026

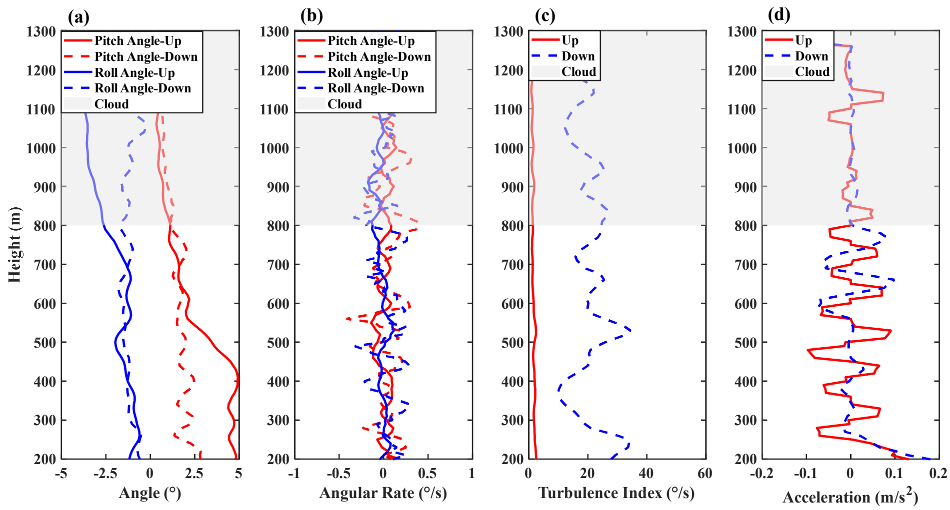

Figure 11. Same as Figure 9, but for the period of 19:43–19:55 BJT on July 31, 2025.

https://doi.org/10.5194/egusphere-2026-4218
Preprint. Discussion started: 4 August 2026

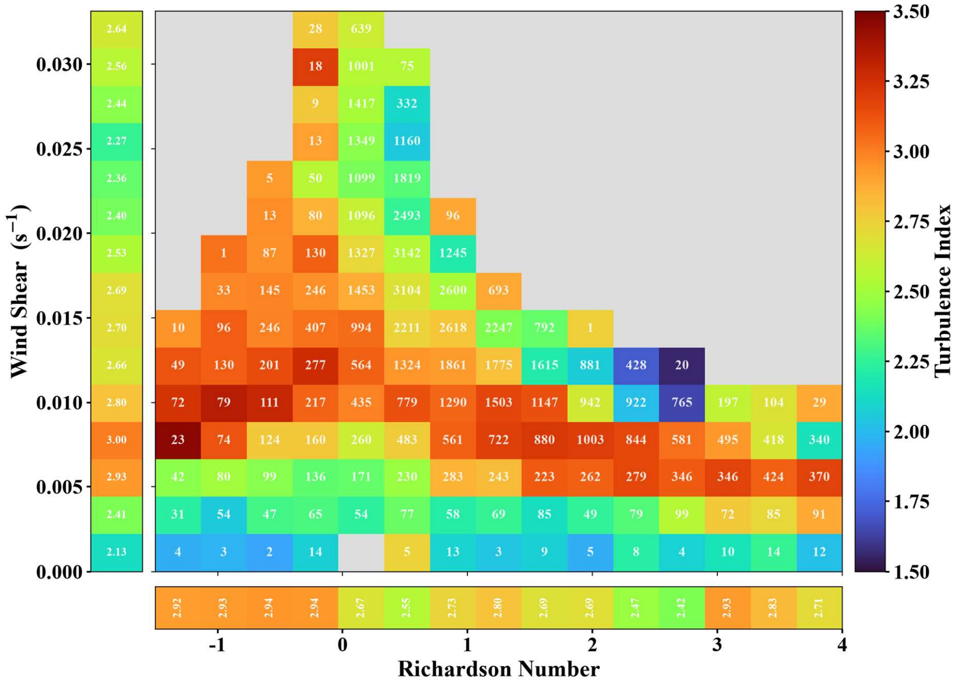

Figure 12. Joint distribution of the gradient Richardson number (*Ri*) and vertical wind shear. The horizontal axis denotes *Ri*; the vertical axis represents vertical wind shear with units of s^{-1}. The color bar on the right indicates the UAV-derived turbulence index (unit: °/s), where higher values indicating stronger atmospheric turbulent disturbances and more intensive UAV flight perturbations, while lower value corresponding to quiescent atmospheric conditions with negligible turbulent interference.